Estimating Missing Line Data in Illuminated Contour-Based Markers

J. C. BARCA, S. W. TENG., and M. MORGAN

***Abstract*-- This paper first describes a new Multicolour Illuminated Contour-based marker, which address the occlusion and identification problems that are associated with current optical motion capture markers. Methods that can be used in conjunction with the new markers to: i) pre-process the marker data, ii) estimate missing marker data, iii) identify the markers, and iv) locate the markers, are then described. Five experiments, which have been conducted to demonstrate how effectively the new markers address the occlusion problem, are then described and the results discussed. The presented work is important because it seeks to improve the current Marker-based optical motion capture technology which is the most accurate and widely used form of motion capture, but which has significant problems in the areas of marker occlusion and marker identification. Solutions to the current problems of marker occlusion and identification can be expected to provide significant benefits for industries reliant on motion capture technology.**

***Index Terms*—Animations, Clustering, Interpolation formulas, Video.**

I. INTRODUCTION

Motion capture is the process of capturing and reconstructing real world movements of one or more subjects. Motion capture has been recognized as an important tool in many areas, such as medical analysis [1], sports [2], and advanced control interfaces, which can be used for tele-manipulation [3]. Optical Motion Capture (OMC) systems can generally be classified into two categories, which are referred to as Marker-based systems and Marker-less systems. In this research, we focus on Marker-based systems because these systems to date are most widely used, and because they are relatively more robust and precise [4], [5].

Marker-based OMC systems use markers and optical cameras to capture the movements of subjects. The systems can track face gestures, skin deformations and skeletal structures. However, this research focuses on tracking skeletal structures as this is most relevant in medical analysis, sports and control interfaces for telemanipulation.

The skeletal structure of a subject can be tracked by first distributing markers onto areas of interest on the subject's body, and capturing video footage of the body as it moves. The positions of the markers are then tracked over time, by repeatedly identifying the 2-dimensional (2D) coordinates of specific features of the markers in the sequences of frames, which constitute the captured video footage. To reconstruct the movement of the subject, the 2D coordinates

identified at each time step are first synthesized into 3-dimensional (3D) coordinates. 3D coordinates from the same markers, are then linked together to form sequences of 3D coordinates, which represent the movements of the subject over time. A sequence of images, which portray an actor who is walking during a classical Marker-based OMC process, is shown in Figure 1.

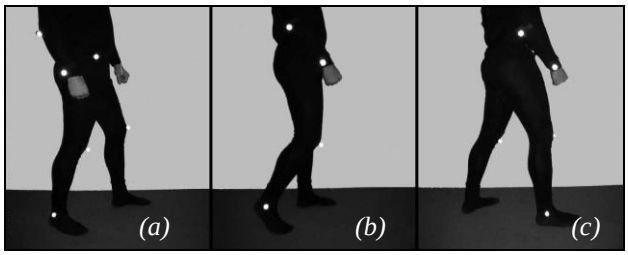

Fig. 1. Actor walking during a classical Marker-based OMC process.

Many different marker designs have been investigated. Some markers are Passive, which means that the identity of one marker on a position of the body cannot be differentiated easily from the markers on other positions of the body. Others are Active, which means that the markers do express their identities explicitly. Examples of different Passive and Active markers include: Passive spherical retro-reflective markers, Active spherical markers with flashing Light Emitting Diodes (LEDs), Active square markers with surface patterns, Active square markers with a single color painted onto their surfaces and Active retro reflective mesh markers. Four of these types of markers are shown in Figure 2.

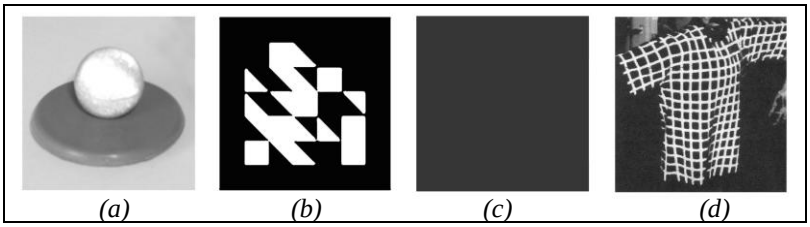

Fig. 2. (*a)* Passive spherical retro-reflective marker; (*b)* Active square marker with surface pattern [6]; (*c)* Active square marker with a single color painted onto its surface [7]; and *(d)* Active retro reflective mesh marker [8].

Current markers have weaknesses, which limit their respective OMC systems' effectiveness and efficiency. Two major weaknesses with current markers are that:

1. their designs restrict the subject's movements;
2. they are not robust against occlusions that block the line of sight between the cameras

and the markers.

As described above, Active markers are designed so that their identity and position on the subject can be tracked more easily compared to Passive markers. However, the designs of current Active markers restrict the subject's movements. For example, the classical Active spherical markers express their identities through flash sequences of various frequencies generated from light-emitting diodes (LEDs) on each marker. To generate various frequencies of the flash sequences and to synchronize the flash sequences with the shutters of the cameras, every marker is connected with a wire to stationary computers. Such connectivity restricts the movement of the subject. This method of expressing the identities of the Active spherical markers also produces large quantities of video frames, which require more time to process them. Instead of using flash sequences, other Active markers use intricate surface patterns [6] or a single color painted onto their surfaces [7] to express their identities. Although there are no wires connecting the markers with computers, the markers with intricate patterns still restrict the subject's natural movements as the markers would need to be closer than 75 centimeters from the capturing cameras for the intricate patterns to be captured accurately. The problem with the latter markers is that they are unable to generate enough identities to track a complete human body, unless constraints are enforced on the movements of the user.

To achieve robust and accurate tracking in OMC systems, occlusion is one of the most significant weaknesses to address [9]-[11]. Occlusions limit the effectiveness and efficiency of OMC systems because they can cause marker data to go missing during the tracking process, and make the task of determining the 3D positions of the tracked markers difficult or impossible in some cases [9], [11]. The two main reasons for why current markers not are robust toward occlusions are: i) the size of current markers is small (e.g. classical spherical markers are only about 2.5 cm in diameter) and they are therefore easily occluded; and ii) when current markers are partially occluded, their designs make the task of estimating marker positions difficult, as the occluded information greatly increases the difficulty of locating features, which can be used to determine where the markers are positioned. Some OMC systems attempt to minimize the number of occlusions by using more markers. Other systems address the problem by using more cameras. However both these approaches greatly increase the quantity of images to process and the complexity of mapping corresponding marker images captured by the cameras. An additional

drawback with adding extra cameras is increased cost of the OMC system.

To address the above weaknesses with current markers, we have designed a new Multicolor Illuminated Contour-based (MIC) marker [12], [13]. Each MIC marker is constructed using intersecting pairs of flexible illuminated glow wires which each are 3 mm thick and 16 cm long. The two wires of a marker are of different colors and the intersection point of the two wires denotes the exact position of a marker on the subject. The glow wires are powered by a battery driven inverter. Two MIC markers and a battery driven inverter is shown in Figure 3.

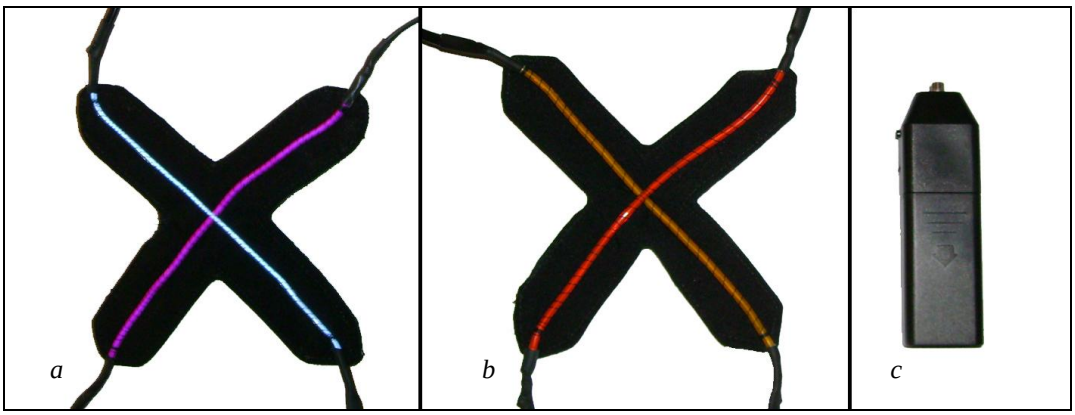

Fig. 3. Two MIC markers and a battery driven inverter. Image *a* shows a purple and turquoise MIC marker, image *b* shows a red and orange MIC marker, and image *c* shows a battery driven inverter.

The use of static color allows the new markers to be identified within one image, rather than through a sequence of images, and this makes it possible to lower processing time. The use of static colors also eliminates the need for wiring the markers to a complex computer in order to trigger flash sequences, or to synchronize the flash sequences with the shutters of capturing cameras. The static colors of our markers also allow them to be correctly identified further from capturing cameras than markers, which use intricate patterns for expressing their identities. When used on a subject, each marker's identity is denoted by a unique color combination of its two glow wires. There are currently 10 glow wire colors available on the market. The combination of two different colors allows up to 55 different identities to be used in the marker system. This is more than enough marker identities to support accurate tracking of human body postures, as it has been shown that a human can be tracked correctly with only 16 different markers [5].

The proposed MIC markers are also designed to address the weaknesses described above due to occlusion. MIC markers are designed to have a larger span as compared to most current markers (e.g. the classical spherical markers) to reduce the chance for markers to be completely

occluded. When a MIC marker is partially occluded, the visible parts of the marker's glow wires not only allow effective estimation of the marker's identity using their colors, the angles in which the visible parts of the two glow wires tend to converge also provide useful information to effectively estimate the marker's position on the subject using intra-frame interpolation methods. Using intra-frame interpolation is more efficient than inter-frame interpolation methods (usually used by current marker systems) because intra-frame method requires data in one frame, rather than much higher volume of data from many frames, to perform various estimations. Furthermore, intra-frame method also does not require mapping of markers from different frames, which is a computational expensive process. If the visible parts of the MIC marker do not provide sufficient information, inter-frame interpolation methods can still be applied to estimate its identity or position.

As the proposed MIC markers have a radically different design than current markers, the OMC processes used to track the markers are also different. In next section, we provide an overview of the processes that are used to track MIC markers in 2D images. Experiments that demonstrate how effectively the MIC markers and the OMC processes address issues related to occlusions, are presented in Section III. Due to page limitations experiments relating to accuracy of marker localization will not be discussed here but rather in a separate paper. Section IV concludes this paper.

II. Major Processes used to Capture and Track MIC Markers

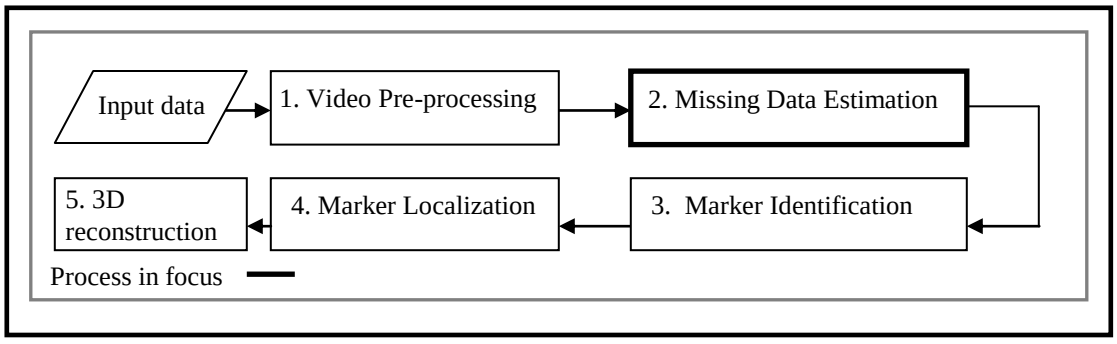

Fig. 4. Main processes used to capture and track MIC markers.

An overview of the main processes that are used to track MIC markers in 2D images is provided in Figure 4. Process 1 to 4 is described in greater detail below. The main focus will be on Process 2, as missing data that is caused by occlusions, can be the main source of error in

Marker-based OMC [9]-[11]. Process 5 will not be discussed in this paper as we use a standard 3D reconstruction process. How 3D reconstruction can be conducted, is described in [14]-[16].

A. Video Pre-processing

The aim of this process is to retain pixels that are related to the MIC markers, and to filter out all irrelevant pixel data. The first step of this process extracts an image from the captured video footage. In the second step, the image is scanned to classify the pixels into separate color channels, which correspond to the colors of the MIC markers. One additional channel is specified which corresponds to irrelevant data. In the final step, a modified K-means filter, developed to process these markers, is used to remove noise in the pixel data that represents the MIC markers [17]. The differences between standard K-means, and the new modified K-means noise filter, are in the processes, which automatically identify clusters with noise and valid data.

- determine how many clusters of valid data an image should have.
- merge clusters that contain data from the same line segment in the same MIC marker.

An overview of the steps involved in the noise filtering process is given in Figure 5. The individual steps are explained in greater detail below.

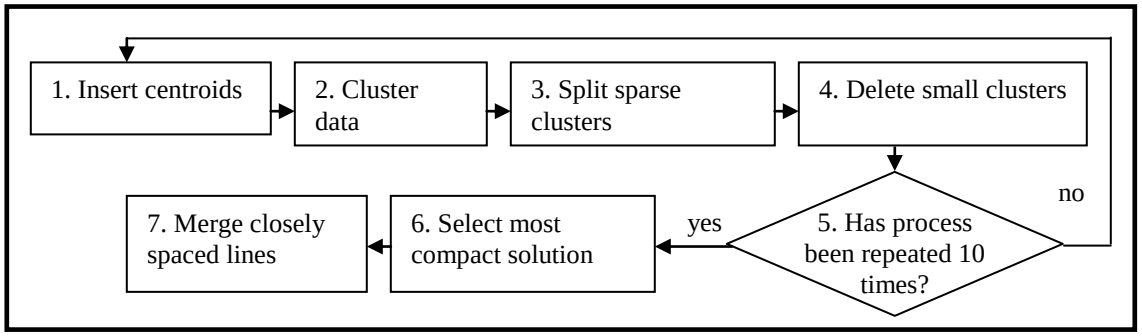

Fig. 5. Overview of the steps involved in the noise filtering process.

To initialize the modified K-means algorithm, two cluster centroids are introduced at pre-defined positions in the image. However, as the algorithm only performs local search, and the determination of initial centroid positions plays a big part in the resulting cluster compositions, the overall clustering process has to be iterated 10 times with 10 different pre-defined initial centroid positions, to make the search mechanism more exhaustive. The pre-defined cluster positions are selected so that the search space is covered as much as possible throughout the 10

runs.

When the centroids have been placed into the image, the modified K-means algorithm cleans up noise by creating clusters of pixels based on their relative spatial positions in the image. Following the classical K-means algorithm the Euclidean distance measure is used to determine which cluster a pixel belongs to. Each pixel is classified to a cluster, which yields the minimum Euclidean distance between the pixel and the respective centroid. The centroid of each cluster is updated iteratively by calculating its new coordinate as the average coordinate of the pixels in the cluster, until it converges to a stable coordinate with a stable set of member pixels.

Cluster compactness is used to determine the optimal number of clusters for a given image. The compactness of a cluster is determined by analyzing the number of pixels located within a rectangular bounding-box, which is defined by the outer bound of the cluster (i.e. the pixels that have the maximum and minimum x and y coordinates respectively). A cluster that has a lower degree of compactness than a specified value will be split. The degree of compactness used is 20%, as it was found empirically that this is a value just below the general minimum compactness of valid marker data in this domain.

A cluster is classified as noise if it only has low number of pixels. The minimum number of pixels in a cluster, or the cluster size, should be set such that it minimizes the degree of false positives (i.e. data clusters incorrectly classified as noise) and false negatives (i.e. noise clusters incorrectly classified as data). The minimum cluster size is domain specific and is determined by observing the number of data points usually found in a noise cluster for the type of data at hand. In this research, the minimum number of pixels in a cluster is set to eight. This was done because empirical results indicated that compact clusters of noise usually contain less than eight pixels, and clusters with valid marker data usually contain more than eight pixels. The clustering, splitting and deleting processes are repeated until the number of clusters stabilizes. When the process has run 10 times the result of the run that produced clusters with the highest total degree of compactness is selected.

In the last step of the clustering process, closely spaced clusters of data that belong to the same line segment are merged. Two clusters are merged if the Euclidean distance between their centroids is within a predefined percentage of the height of the image at hand. The percentage of the image height was used, as this makes it possible to scale the defined distance automatically

when different image sizes are used. The percentage was set to 15 percent based on empirical trials.

B. Missing Data Estimation

The processes involved in finding and estimating intra-frame MIC marker data, which has been lost due to occlusions, is described in detail in this Section. The processes used to estimate missing data in MIC markers and classical spherical markers are fundamentally different. This is mainly due to the different types of features that are used to locate them (e.g. the intersecting point of line segments are used to locate MIC markers and the aim of the processes, which are used to estimate missing data in these markers, is therefore to find missing line data. In traditional spherical markers on the other hand, the center point of their spherical shape is used as a means to locate the markers. The aim of the processes that are used to estimate missing data in these markers, is therefore to obtain information, which can be used to determine the center point of spherical shapes). An overview of the processing steps that are used to find and estimate missing MIC marker data is shown in Figure 6, and each process is described at greater length below.

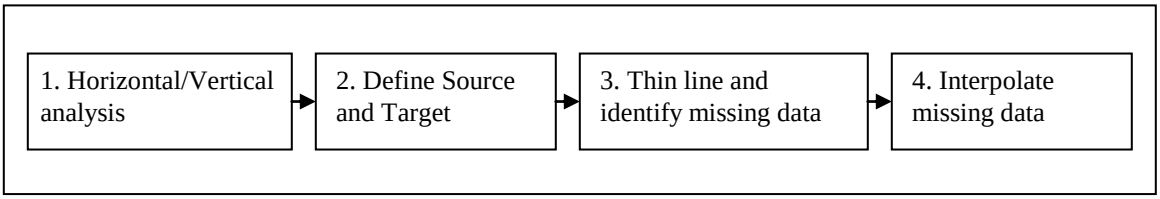

Fig. 6. Processes involved in finding and estimating missing intra-frame MIC marker data.

1) Horizontal/Vertical Analysis

The Horizontal/Vertical (HV) analysis is required due to the nature of the MIC markers and is conducted to obtain knowledge that can act as a guide for further processing. To conduct this analysis, each line segment in an image is encapsulated into a bounding box. If the image pixels of the line fit into a box with a greater horizontal than vertical length, then the line is regarded as being horizontal. If the bounding box has a greater vertical than horizontal length or the vertical and horizontal lengths are the same, then the line segment is regarded as being vertical. An example of a horizontal line is illustrated in Figure 7.

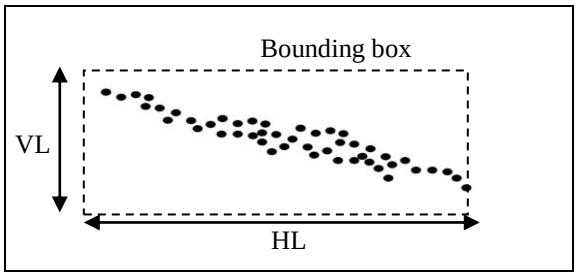

Fig. 7. Bounding box, where VL < HL, defining the line as horizontal. VL is the vertical length and HL is the horizontal length of the bounding box.

2) Definition of Source and Target

Results from the HV analysis are used to assist in the determination of Source and Target points for each line. If a line has been found to be horizontal, the image pixels within the processed line with the minimum and maximum *x* pixel coordinate values are selected as Source and Target points. If a line has been defined as vertical, then the image pixels with minimum and maximum *y* coordinates are selected. Source and Target points for the horizontal line displayed above are illustrated in Figure 8.

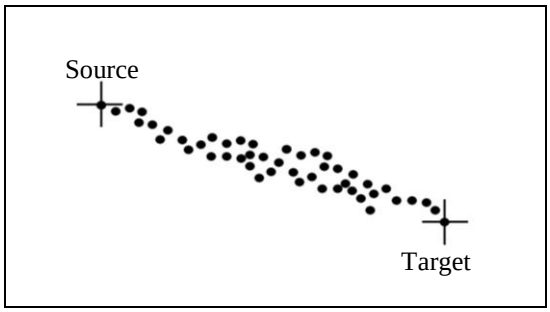

Fig. 8. A horizontal line with defined Source and Target points.

3) Line Thinning

To define the line that best fits the raw line segment data, a search that tracks and thins the raw data into a 1 pixel wide line is propagated from Source to Target. This thinning process constructs a new line by progressively moving a pixel unit from Source to Target, constructing a segment of the new line along the way. For constructing each segment, the average coordinate is derived from image pixels in *y* direction if the line is horizontal, whereas the average coordinate is derived from image pixels in *x* direction if the line is vertical. The thinning procedure also identifies if there is any missing data in the raw line. Figure 9 shows the line constructed by the thinning procedure using the points shown in Figure 8.

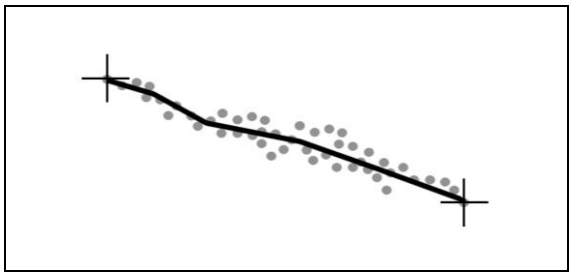

Fig. 9. A thinned horizontal line.

4) Intra-frame Interpolation of Missing Data

If a region with missing line data is detected during the thinning process, then an intra-frame interpolation algorithm is initiated. Intra-frame interpolation is used because [18] indicates that data is estimated more accurately by using interpolation than by using extrapolation, and more accurately intra-frame than inter-frame. This focus is also held because techniques, which supports accurate intra-frame interpolation naturally also supports improved inter-frame interpolation.

The presented interpolation algorithm uses a combination of Moving Average (MA) and Inverse Distance Weighted Interpolation (IDWI) to estimate the missing pixel data. We named this hybrid algorithm MA-IDWI. This hybrid interpolation algorithm can exploit knowledge stored in multiple known data points in order to accurately estimate missing data in MIC markers, if multiple data points are available on each side of the missing line data. This gives MA-IDWI an edge over IDWI, as the latter is unable to make use of knowledge from more than two known data points in the interpolation process. MA-IDWI can also estimate missing data in MIC markers if only one known data point is available on each side of the missing line data, and this is not possible with traditional MA algorithms. The hybrid interpolation algorithm is therefore more flexible than both traditional MA and traditional IDWI interpolation algorithms.

To estimate missing data in MIC markers, the hybrid MA-IDWI interpolation algorithm first tries to interpolate the missing line data using MA, and a search ellipse is therefore defined. This search ellipse encapsulates the area with missing line data, and two autoregressive half-plane models (HPMs) located on each side of the missing data, which are fitted with known data. We chose to use an ellipse size, which encapsulates the region with missing data and two HPMs that each incorporates four known pixel coordinates. The researchers chose to incorporate four known pixel coordinates into each HPM, because literature indicates that the greatest improvements are

achieved when the number of known coordinates is increased from 1 to 4 [19]. The search ellipse is illustrated in Figure 10. HPM1 is the half plane model located before the missing data and HPM2 is the half plane model located after the missing data. $x_1, x_2 ... x_i$ are known pixel coordinates fitted to HPM1, $y_1, y_2 ... y_i$ are known pixel coordinates fitted to HPM2 and $\hat{\rho}_1, \hat{\rho}_2 ... \hat{\rho}_i$ is the missing data.

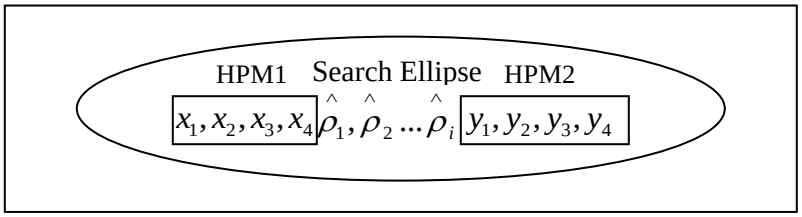

Fig. 10. Search ellipse used in the MA component of the hybrid intra-frame interpolation algorithm.

If enough known data is available to fill both HPMs, then the HPM fitted with image pixels with lowest *x* or *y* coordinate values (depends on results from HV analysis) is used to calculate angle values α_1, α_2 and α_3 between pairs of consecutive image pixels within the relevant HPM (e.g. if the line is horizontal the HPM with the lowest *x* coordinate values is used to calculate angle values, otherwise the HPM with lowest *y* values is used). The selected HPM calculate the angular values by first analyzing the relationship between the pair of image pixels located furthest away from the missing data and incrementally analyzing the relationship between pairs of image pixels while moving towards the region with missing data. In an HPM fitted with pixel coordinates x_1, x_2, x_3 and x_4, and where pixel coordinate x_1 is located furthest away from the missing data (as in Figure 10), angle value α_1 refers to the relationship between pixel coordinates x_1 and x_2. Angle value α_2 refers to the relationship between pixel coordinate x_2 and x_3, and angle value α_3 refers to the relationship between pixel coordinate x_3 and x_4.

To describe the angular relationship between two pixel coordinates, each of the angle values α_1, α_2 and α_3 are associated with an expression containing two numbers. An example of such an expression is (–1, 1). The first number in this expression refers to the relationship between the two pixels in *x* direction, whereas the second number refers to the relationship in *y* direction. A mapping model that shows how relationships between pairs of pixels are expressed is shown in Figure 11. In this model, the pixel located furthest away from the missing data is

located in the grid unit labeled (0, 0). The image pixel one step closer to the missing data is located in one of the surrounding grid units.

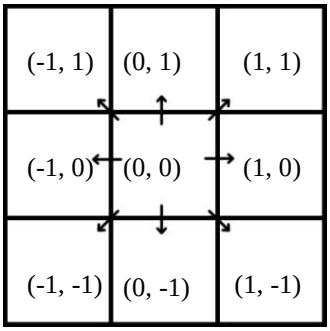

Fig. 11. How angular relationships between pairs of image pixels are expressed.

An α with values (-1, 1) would therefore refer to a relationship between two pixels where the pixel located closest to the missing data is found to the upper left from the pixel located furthest away. When angular values α_1, α_2 and α_3 have been found (as in HPM1 in Figure 12), the average angle between the pixels is calculated. This average angle is then used to guide the interpolation of the missing pixel located closest to the relevant HPM. In the case of the example illustrated in Figure 12, this would mean that interpolated pixel I_1 would substitute $\hat{\rho}_1$.

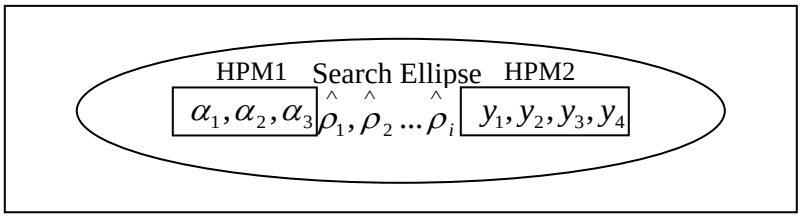

Fig. 12. Angular values α_1, α_2 and α_3 has been calculated in HPM1.

If there still is missing data in the search ellipse after this first pixel has been interpolated, then the HPM fitted with data points with largest *x* or *y* pixel coordinate values is used to interpolate the next pixel I_2. This would in the given example mean that $\hat{\rho}_i$ would be substituted with I_2 (see Figure 13).

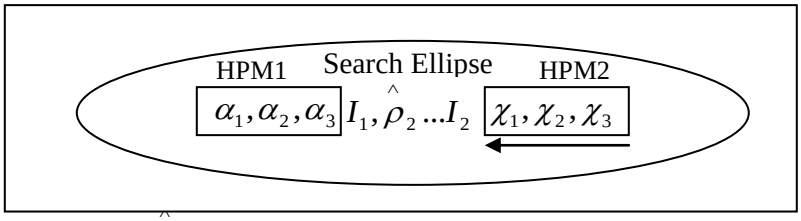

Fig. 13. Missing pixel $\hat{\rho}_i$ has been interpolated using the average angle of χ_1, χ_2 and χ_2 in HPM2.

To interpolate all missing data in a search ellipse, the MA algorithm alternates between using each of the two HPMs for interpolating the missing data. This is done by iteratively updating the relevant HPM by removing the known pixel coordinate located furthest away from the missing data and including the newly interpolated point.

If there not is enough known data available to fill both HPMs, then IDWI is used for interpolation instead of MA. The benefit of using IDWI in these cases is that IDWI only requires one known pixel coordinate from each side of the region with missing line data, to interpolate the missing information. The formula used by the IDWI component of the hybrid interpolation algorithm is presented in (2).

To interpolate the 2D coordinates of the pixels, which forms the missing line data, the IDWI algorithm starts off by substituting K_b with the *x* or *y* value from the known pixel coordinate with the lowest *x* or *y* value (as in MA the dimension depends on results from the HV analysis). K_a is substituted with the *x* or *y* value from the known pixel coordinate with the highest *x* or *y* value. The IDWI algorithm then progress by counting the number of pixel units located between K_b and K_a. This number is used to calculate how many percent one pixel unit constitute, of the total size of the region with missing line data. P is then substituted with this percent value, and the missing one dimensional coordinate value calculated according to the Equation 1. To calculate the second dimension of the 2D coordinate, the process is repeated for the second dimension. The resulting 2D coordinate is used to interpolate a pixel into the pixel unit located closest to the known pixel coordinate, with the smallest *x* or *y* coordinate value. To interpolate all the missing line data the process is repeated until the end of the hole is reached.

$$M = \left(K_a - K_b\right)\frac{P}{100} + K_b \tag{1}$$

where:

M : One dimension of missing pixel coordinate
K_b : One dimension of known pixel coordinate located before missing data
K_a : One dimension of known pixel coordinate located after missing data
P : Pixel unit number between K_b and K_a

C. Marker Identification

The marker identification process is necessary in order to: i) determine the location of different body parts, ii) achieve correspondence between the tracked body parts and the objects used to reconstruct the captured movement, and iii) to recognize body parts over time. We conduct marker identification by first grouping closely spaced pairs of line segments with different colors into markers (a separation of 20 pixel units or less has empirically been found to produce good results on the processed datasets). The markers are then labeled according to the colors of the of line segments constructing them. If a line segment is located further than 20 pixels units away from all other segments of different colors, then the line segment is discarded from further processing.

D. Marker Localization

The marker localization process is conducted to determine where in the captured images particular markers are located. We localize markers by analyzing each marker in an image separately. The process is initiated by propagating a search up the line segment with the smallest x coordinate value. The search starts from the end of the line with smallest x coordinate values if the line was found to be horizontal, and the end of the line with the smallest y coordinate values if the line was found to be vertical. The search propagates through line segments in increments of five pixel units. Increments of five pixel units are used because this number has been found empirically to produce a good trade off between accuracy and processing speed. The aim of the search process is to first find pixels within the second line of the marker, that are located less than 10 pixel units away. When a pixel that is located less than 10 pixel units away is found, a "fine search" procedure is initiated. This "fine search" procedure aims to find pixels within the second line of the marker, which are closer than five pixel units away, and propagates through the line in one step increments rather than in five step increments. Pixels that are located less than five pixel units away are stored and their mean coordinate used to determine the location of the marker. The process is repeated for all markers in the dataset.

III. Experimental Design and Results

Four experiments are presented in this section. All these experiments investigate how robust the new MIC markers and the processes that are used to track them are towards occlusions. The focus is still set on the occlusions problem, because this problem is one of the most significant problems for Marker-based OMC today [9]-[11].

The first experiment compares the performance of the devised hybrid MA-IDWI interpolation algorithm with the following algorithms: Grid Filling (GF), Manhattan Routing (MR), four-layered Non-Manhattan Routing (Non-MR), and Bézier splines (B-splines). The MA-IDWI algorithm is compared to these alternative algorithms, because literature states that they have been successfully used to generate lines between known 2D points. (Good descriptions of GF can be found in [20], [21], while thorough descriptions of MR are given in [22], [23], Non-MR is described in detail in [27], [25], and descriptions of B-splines are provided in [26], [27].) This experiment evaluates how accurately the different algorithms interpolate missing line data intra-frame, as line segments with missing data are increasingly bent. The second experiment measures how large occlusions that can be located directly above the intersecting point of line segments in MIC markers, before we are unable to identify and locate the markers. The last two experiments directly compare how many occlusions that are generated when MIC markers and traditional spherical markers, which are used by state of the art Marker-based OMC systems such as Vicon, are worn by a human subject. We do not compare the MIC markers to the other marker systems that have been discussed in this paper as spherical markers are most widely used.

All the image data that was processed in these experiments was captured with optical video cameras. The images include MIC markers of different colors, and they have an identical size of 720x576 pixels and a resolution of 72 pixels per inch. The image format is BMP. All image data was pre-processed with the methods described in Section II, before the experiments were conducted.

The MIC markers, and names of all methods that have been used in the motion capture system, are referred to in *Italics* throughout the remaining parts of this paper. This is done to make it easy to distinguish between the technologies that have been devised as part of this research, and the existing technologies that are used to compare their performance.

A) Comparing the Performance of Interpolation Techniques as Line Segments with Missing Data are Increasingly Bent

This experiment explores how accurately *MA-IDWI*, MR, Non-MR, GF, and B-splines recreate missing data in increasingly bent line segments. To investigate this is important, as the line segments will have some degree of bending most of the time when the *MIC markers* are attached to a human body. To investigate the issue, an illuminated line segment was captured onto images 12 times, while it was increasingly bent. For each run the bending was increased with 10°, starting with 0° in run one, and ending at 110° in run 12. 30 known data points were then removed from the line segment in each of the captured images. This removed data was used as ground truth. The missing data was then interpolated with each of the interpolation algorithms.

The results produced by each interpolation algorithm are presented in Figure 14. One can observe that the results are comparable when there is a small amount of bending, and that *MA-IDWI* produced the best results in all runs when the bending was increased beyond 70°. One can also observe that there are large deviations in the quality of the results produced by MR. These large deviations occur, because the quality of the results depend on how the corners of the rectilinear lines (produced by MR) align with the bending of the line segment (see Figure 15). Known data is plotted as black continuous lines, ground truth data is represented by gray continuous lines, and the rectilinear lines generated by MR is shown as black stippled lines. One can observe that the discrepancy between the rectilinear line and the ground truth data, is small in line *a*, where the corner of the rectilinear line is aligned with the bending of the line segment. One can also observe that the discrepancy is large in line *b*, were the corner of the rectilinear line not is aligned with the bending of the line segment.

The mean ASE produced throughout the experiment is shown in Figure 16. One can observe that *MA-IDWI* produced the best overall results with a mean ASE of 99.72 pixel units from ground truth. One can also observe that B-splines produced the second best overall result with a mean ASE of 138.09. This shows that there is a clear difference between the mean results produced by the two algorithms, as B-splines generated a mean ASE of 38.37 more than *MA-IDWI*. This therefore shows that *MA-IDWI* was a good choice. The three remaining algorithms produced poorer results. MR produced a mean ASE of 181.81, which is an ASE of 43.72 pixel units more than the mean ASE produced by B-splines. Non-MR produced similar results as MR,

with a mean ASE of 184.18. GF produced the worst overall result, with a mean ASE of 205 pixel units from ground truth.

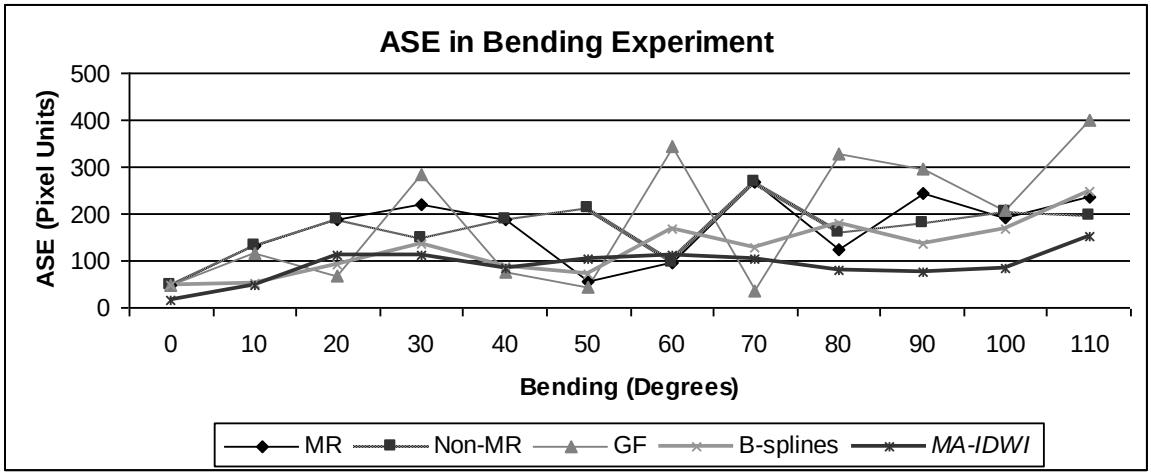

Fig. 14. Errors as the amount of bending increases.

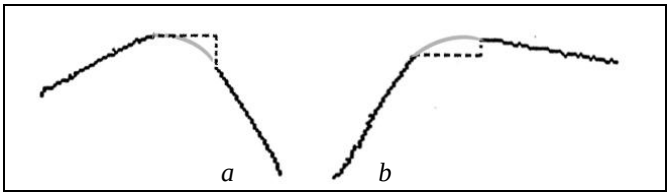

Fig. 15. Difference in quality of results when MR is used.

Mean ASE in Pixel Units				
MA-IDWI	B-splines	MR	Non-MR	GF
99.7	138.1	181.8	184.2	205

Fig. 16. Mean ASE in the line bending experiment.

B) Tolerated Size of Marker Occlusions

This experiment was designed to measure how large occlusions can be before we are unable to correctly identify and locate the markers when the occlusion is located directly above the intersecting point of line segments in *MIC markers*. Six different *MIC markers* were mounted on a flat board to prepare for data collection. Square occlusions of 0.5 square centimeters were then placed on top of the intersection point of the line segments in the *MIC markers*. The six MIC markers were then captured five times onto different images while the board they were mounted on was moved to random positions from the capturing camera, with the minimum distance being

one meter away and the maximum distance being five meters away. This process was repeated 15 times with the size of the square objects increasing from 0.5 cm² to 7.5 cm² across runs (width and length of the objects was incrementally increased with 0.5 cm). This resulted in a total of 450 processed markers for this experiment. Results from this experiment are presented in Figure 17.

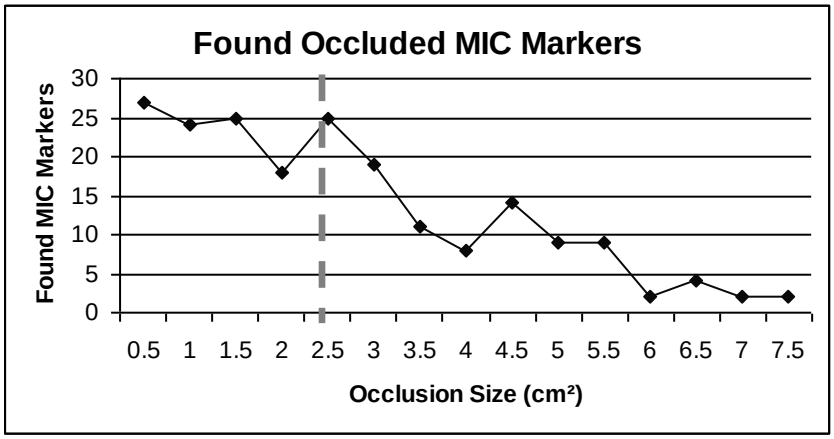

Fig. 17 Correctly found *MIC markers* as the size of occlusions increases.

One can observe that the number of correctly processed markers naturally decreases as occlusion sizes increase, and that 63.33% of the 30 *MIC markers* still are correctly identified and located when the occlusion size is 3 cm². This is a good result compared to results displayed by traditional spherical markers, as these typically are 2.5 cm in diameter and therefore would have been completely hidden by this kind of occlusion. (It is impossible to locate traditional spherical markers such as the ones used by Vicon intra-frame, when occlusions have a size beyond the vertical gray dashed line displayed in Figure 17.) One can also observe that approximately one third of the *MIC markers* are correctly processed when the size of the occlusions is 5 cm². When occlusions of 7.5 cm² were introduced, the marker identification and localization algorithms still managed to process two of 30 markers correctly. This shows that the new *MIC markers* and the devised processing methods, support correct processing when occlusions are three times larger than the size of the markers used by state of the art Marker-based OMC systems such as Vicon. This in turn proves the feasibility of using *MIC markers* when there are large occlusions.

C) Robustness toward Occlusions when a Subject Walks Straight

This experiment was designed to investigate if the new *MIC markers* generate fewer occlusions than traditional spherical markers such as the ones used by Vicon, when a human subject walks

in a straight line. A marker is regarded as being occluded if no part of it can be observed in a captured image. The experiment was conducted by first distributing 16 different *MIC markers* onto key positions of a human body. The body then walked straight through a scene surrounded by four cameras in one complete walk cycle, while video footage was captured at 24 frames per second (fps) from all four cameras. When the video footage had been captured, the *MIC markers* were replaced with spherical markers and the process was then repeated. (The spherical markers were positioned at the exact same locations as the *MIC markers*.)

The number of occlusions that were generated in the camera system, as the body walked through the scene, is shown in Figure 18. Each graph has been generated from data captured across 79 time steps, as it took 3.3 seconds for the human subject to walk through the scene. A total of 316 images have therefore been analyzed to generate each graph, as four images were captured at each time step. One can observe that the *MIC markers* generated the lowest number of occlusions throughout the capturing process. This strongly indicates that the *MIC markers* are more robust towards occlusions than classical spherical markers, when they are used to capture normal human gait. The mean number of occlusions also strongly indicates that this is the case, as an average of 25.7 occlusions were generated per time step when *MIC markers* were used, and an average of 34.7 occlusions were generated when classical spherical markers were used. This is an average difference of nine occlusions per time step.

A T-test was conducted to investigate the statistical significance of the results. A null hypothesis, which assumes that there is no difference between the compared results, was used. The results are significantly different if this null hypothesis can be rejected. To determine if equal or unequal variance should be assumed in this T-test, an F-test is conducted. F-test shows that the variance in the dataset generated by the spherical markers is 9.321, and the variance in the dataset generated by the *MIC markers* was 1.813. As a result, unequal variance is assumed when conducting T-test. The T-test was conducted at a confidence level of 0.05. This implies that the null hypothesis could be rejected if the generated probability (P) value was below 0.05. Otherwise, the difference between the results would be considered insignificant.

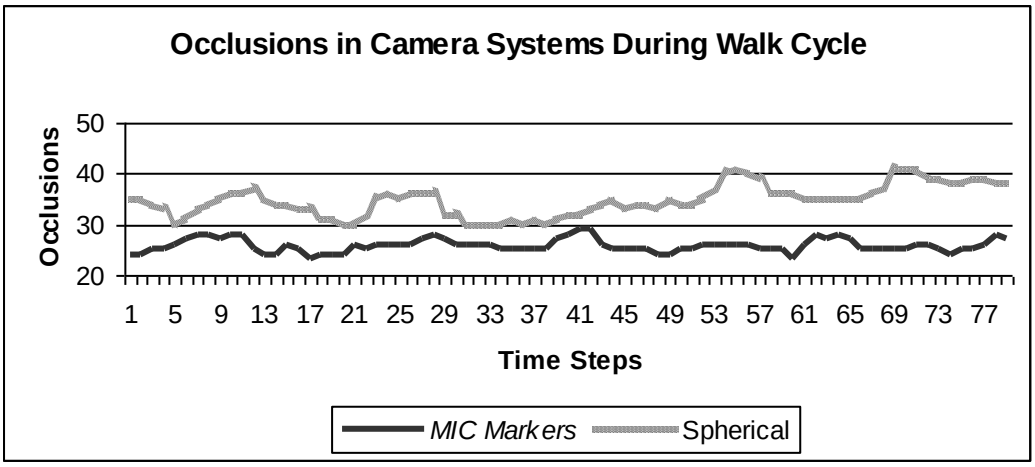

Fig. 18. Number of occlusions when a human body walks straight.

Results from the T-test are shown in Table 1. The two-tailed P value is shown in the shaded region. The null hypothesis can therefore be rejected. As a result, one can say that there is a significant amount of statistical evidence, which points out that *MIC markers* generate fewer occlusions than classical spherical markers, when a human subject walks straight through a scene.

TABLE I
RESULTS FROM T-TEST.

	Spherical Markers	***MIC Markers***
Mean	34.683	25.734
Variance	9.321	1.813
Observations	79	79
Degrees of freedom	107	
t Stat	23.837	
P(T<=t) two-tail	1.314E-44	

D) Robustness toward Occlusions when a Subject Walks in a 8 Shape

This experiment is designed to investigate if the *MIC markers* generate fewer occlusions than classical spherical markers, when a human subject walks through the capturing volume in a path that resembles a figure-of-8 shape. A marker is regarded as being occluded if no part of it can be observed in a captured image at hand. The experiment was conducted by first distributing 16 different *MIC markers* onto key positions of a human body. The subject then walked through a scene surrounded by four cameras in a path that resembled a figure-of-8 shape, while video footage was captured at 24 fps from all cameras. When the video footage had been captured, the subject was equipped with traditional spherical markers before the process was repeated. The

spherical markers were positioned at the exact same locations as the *MIC markers* to ensure validity of the experiment.

The number of occlusions that were generated in the camera system as the subject walked through the scene is shown in Figure 19. Each graph is generated from data that has been captured over 223 time steps, as it took 9.29 seconds for the body to move through the scene. A total of 889 images were therefore analyzed to generate each graph, as four images were captured at each time step. When one inspects the graphs, one finds that the number of occlusions in general was lowest when *MIC markers* were used. This finding is verified when one calculates the average number of occlusions, as the mean number of occlusions per time step was 28.68 when *MIC markers* were used, and 32.34 when classical spherical markers were used. This shows that *MIC markers* can generate fewer occlusions than classical spherical markers, when a human subject walks in a path that resembles an 8 shape.

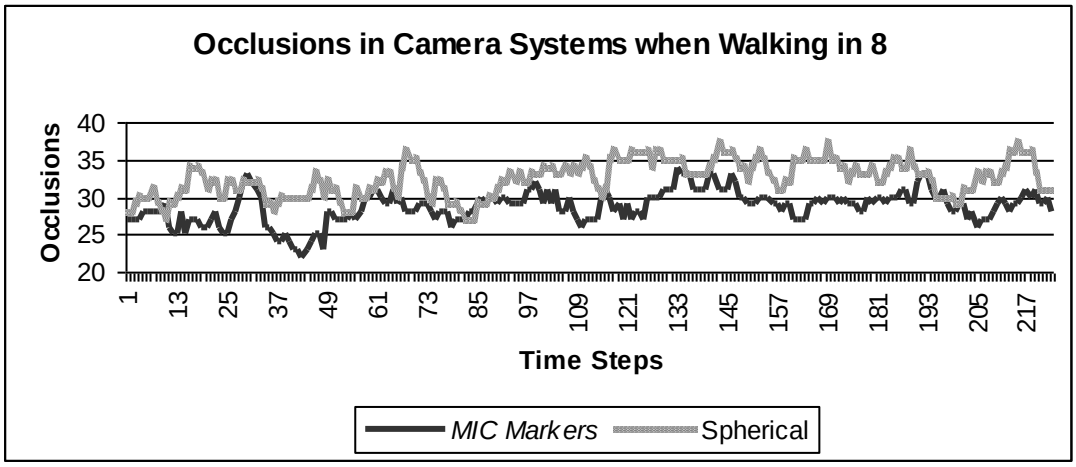

Fig. 19. Number of occlusions when a human body walks in a path that resembles an 8 shape.

A T-test was conducted to investigate if the difference between the generated results is significant. As in the previous experiment, a null hypothesis was employed. A T-test that assumes un-equal variance was used, as an F-test showed that the variance in the dataset generated by spherical markers is 4.261, and the variance in the dataset generated by *MIC markers* is 5.66. Results from the T-test are shown in Table 2. The two-tailed P value is displayed in the gray shaded region. One can observe that the P value is close to zero and the null hypothesis can therefore be rejected. This implies that there is a significant statistical difference between the numbers of occlusions that are generated by the two marker systems. One can therefore say that it is statistically proven that *MIC markers* produced significantly fewer

occlusions than classical spherical markers, when the subject walked through the capturing volume in a path that resembles an 8 shape.

TABLE II
RESULT FROM T-TEST.

	Spherical Markers	***MIC Markers***
Mean	32.349	28.686
Variance	5.660	4.621
Observations	223	223
Degrees of freedom	440	
t Stat	-17.061	
P(T<=t) two-tail	1.83E-50	

IV. CONCLUSION

A set of new *MIC markers*, which address the occlusion and marker identification problems that are associated with current OMC markers, have been described in this paper. Methods that can be used to process data from the new *MIC markers* have also been presented. The presented methods can: i) pre-process *MIC marker* data, ii) estimate missing *MIC marker* data, iii) identify *MIC markers*, and iv) locate *MIC markers* in 2D images. Four experiments were conducted to demonstrate how effectively the new technology addresses the occlusion problem. These experiments showed that: i) *MA-IDWI* recreated missing data in bent line segments more accurately than all the other evaluated interpolation algorithms, ii) 63.33% of 30 *MIC markers* can be correctly processed, when occlusions are so large that classical spherical markers are completely occluded, iii) *MIC markers* generated significantly less occlusions than classical spherical markers when a subject walked straight, and iv) *MIC markers* generated significantly less occlusions than classical spherical markers when a subject walked in a path that resembles an 8 shape. This shows that the new *MIC markers* reduces the occlusion problem associated with classical OMC markers, and that the devised hybrid *MA-IDWI* interpolation algorithm is ideal for estimating missing data in *MIC markers*. These findings are important for the whole field of motion capture, because Marker-based OMC currently is the most accurate form of motion capture, and the occlusion problem is one of the most central problems for Marker-based OMC.

V. ACKNOWLEDGMENT

We gratefully acknowledge the ideas contributed by Dr Raymond Li and Dr Grace Rumantir in the initial stages of this research.

REFERENCES

[1] Jobbagy, A., Komjathi, L., Furnee, E. & Harcos, P. 2000, 'Movement Analysis of Parkinsonians', *Proceedings of 22nd Annual EMBS International Conference*, Chicago, pp. 821-824.

[2] Conley, R., Tulchin, K., Harris, G., Smith, P., Humm, J. & Hassani, S. 2000, 'Pediatric Sports Medicine: An evolution of Applications of Motion Analysis', *Proceedings of Pediatric Gait, 2000. A new Millennium in Clinical Care and Motion Analysis Technology*, Chicago, pp. 116-123.

[3] Redert, P. 2000, *Multi-viewpoint systems for visual 3-D communication*, PhD thesis, Delft Technical University, Delft.

[4] Nakamura, Y., Yamane, K. & Tanie, H. 2008, 'Motion Capture System and Method for Three-Dimensional Reconfiguring of Characteristic Point in Motion Capture System', European Patent Office, international patent number: PCT/JP2006/307677.

[5] Aggrwal, K. & Cai, Q. 1999, 'Human Motion Analysis: A Review', *Proceedings of Nonrigid and Articulated Motion Workshop*, San Juan, pp. 90-102.

[6] Kawano, T., Ban, Y. & Uehara, K. 2003, 'A Coded Visual Marker for Video Tracking System Based on Structured Image Analysis', *Proceedings of the 2nd IEEE and ACM International Symposium on Mixed and Augmented Reality*, Washington, pp. 262-263.

[7] Zheng, K., Zhu, Q., Zhuang, Y. & Pan, Y. 2001, 'Motion Processing in Tight-Clothing Based Motion Capture', *Robot Vision*, Auckland.

[8] Tanie, H., Yamane, K. & Nakamura, Y. 2005, 'High Marker Density Motion Capture by Retroreflective Mesh Suit', *Proceedings of IEEE International Conference on Robotics and Automation*, Barcelona, pp. 2884-2889.

[9] Gutemberg, B. & Guerra-Filho, I. 2005, 'Optical Motion Capture: Theory and Implementation', *Journal of Theoretical and Applied Informatics*, vol.12, no. 2, pp. 61-89.

[10] Silaghi, M., Plankners, R., Boulic, R., Fua. P. & Thalmann, D. 1998, 'Local and Global Skeleton Fitting Techniques for Optical Motion Capture', *Proceedings of Workshop on Modelling and Motion Capture Techniques for Virtual Environments*, Geneva, pp. 26-40.

[11] Chen, X. & Davis, J. 2000, 'Camera Placement Considering Occlusion for Robust Motion Capture', paper presented to Stanford Computer Graphics Lab, Stanford University.

[12] Barca, C., Rumantir, G. & Li, R. 2006, 'A New Illuminated Contour-Based Marker System for Optical Motion Capture', *Proceedings of IEEE Innovations in Information Technology*, Dubai, pp. 1-5.

[13] Barca, C. & Rumantir, G. 2008, 'Illuminated Contour-Based Markers and Noise Filtering', *Computational Intelligence in Multimedia Processing*, Atafi, A., Kacprzyk, J. & Abraham, A. (eds.) Springer, Berlin, pp. 167-189.

[14] Tang, L., Wu, C., Tsui, H. & Liu, S. 2003, 'Algorithm for 3D reconstruction with both visible and missing data', *IEEE Electronic Letters*, vol. 39. no. 23, pp. 1640-1642.

[15] Kang, K. & Heesung, J. 2003, 'Realistic 3D Reconstruction from an Image Sequence', *Proceedings of 7th Korea-Russia International Symposium*, Korus, pp. 126-128.

[16] Abche, A., Tzanakos, G. & Tzanakou, E. 1992, 'A New Method for Multimodal 3-D Image Registration with External Markers', *Engineering in Medicine and Biology Society*, vol. 14, Oct.-Nov., pp. 1881-1882.

[17] Barca, C. & Rumantir, G. 2007, 'A Modified K-means Algorithm for Noise Reduction in Optical Motion Capture Data', *Proceedings of 6th IEEE International Conference on Computer and Information Science*, Melbourne, pp. 118-123.

[18] Barca, C. 2009, *New Multicolour Illuminated Contour-based Markers and their use in Motion Capture*, PhD thesis, Monash University, Melbourne.

[19] Wongwirat, O. & Ohara, S. 2005, 'Moving Average based Adaptive Cuffer for Haptic Media Synchronization in Telehaptics', Proceedings of *IEEE International Conference on Advanced Intelligent Mechatronics*, Monterey, pp. 1305-1311.

[20] Lee, C. 1961, 'An algorithm for path connection and it's applications', *IRE Transactions on Electronic Computers*, vol.10, pp. 346-365.

[21] Hadlock, F. 1977, 'A shortest path algorithm for grid graphs', *Networks*, vol.7, pp. 323-334.

[22] Mikami, K. & Tabuchi, K. 1968, 'A computer program for optimal routing of printed circuit connectors', *Proceedings of IFIP*, pp. 1475-1478.

[23] Hightower, W. 1969, 'A solution to line-routing problem on the continuous plane', *Proceedings of 6th Design Automation Workshop*, New York, pp. 1-24.

[24] Koh, C. & Madden, P. 2000, 'Manhattan or Non-Manhattan? A Study of Alternative VLSI Routing Architectures', *Proceedings of Great Lakes Symposium on VLSI*, Evanston, pp. 47-52.

[25] Stan, M., Hamzaoglu, F. & Garret, D. 2004, 'Non-Manhattan Maze Routing', *Proceedings of 17th Symposium on Integrated Circuits and Systems Design*, Pernambuco, pp. 260-265.

[26] Lee, S. & Paik, K. 1993, 'Image Interpolation Using Adaptive Fast B-Spline Filtering', *IEEE International Conference on Acoustics, Speech, and Signal Processing*, Minneapolis, pp. 177-180.

[27] Cross, A. & Hancock, E. 1999, 'Extracting curvilinear features from millimetre radar data', *Proceedings of 7th International Conference on Image Processing and Its Applications*, Manchester, pp. 537-541.